Quantum dynamics under the influence of external magnetic fields

S. Midgley* and J. B. Wang†
Department of Physics, The University of Western Australia, Perth 6907, Australia
(Received 16 January 2002; revised manuscript received 7 January 2003; published 11 April 2003)

In this paper, we describe a very versatile numerical model, which can be applied to study the quantum dynamics of an electron wave packet in the presence of external electric and magnetic fields. Detailed numerical analysis is carried out in the paper on the validity of such a model, including (1) comparison with analytical solution in the case of uniform magnetic field, and (2) stringent numerical tests in the case of both electric and magnetic fields. The algorithm presented here is found to be highly accurate, computationally efficient, and numerically stable. It also has the advantage of being able to accommodate arbitrarily complex magnetic field profiles as well as time-varying external fields.

DOI: 10.1103/PhysRevE.67.046702 PACS number(s): 02.70.−c, 31.15.−p, 73.23.Ad, 73.23.−b

I. INTRODUCTION

The transport of two-dimensional (2D) electrons under the influence of an external magnetic field has attracted considerable interest recently, showing a range of interesting phenomenon with promising novel applications. For example, it has been used to probe nanostructured devices for impurities [1], to study quantum ratchets [2] and quantum chaos [3], and to understand the interference of different electronic paths [4]. While many experiments have been performed, a fully quantum mechanical model to describe the various systems involving external magnetic fields has not been available, especially for nonuniform and time-varying fields. Many classical and semiclassical models have been developed (for example, see Refs. [1–5]), but these fail to capture the full quantum nature of the physical systems at the nanometer scale. As an example, Koonen *et al.* [1] used a rather crude model in the analysis of their experimental data, which artificially cuts off parts of a wave function blocked by an electric potential. In their paper, they called for a more sophisticated model to help building a detailed picture of the shape and size of the density fluctuation in a 2D electron gas.

A full quantum mechanical treatment requires an accurate solution of the corresponding time-dependent Schrödinger equation, which reads

$$i\frac{\partial\psi(\mathbf{r},t)}{\partial t}=\mathcal{H}\psi(\mathbf{r},t), \tag{1}$$

where the system Hamiltonian is

$$\mathcal{H}=-\frac{1}{2m}(-i\boldsymbol{\nabla}-e\mathbf{A})^2+e\mathcal{V}, \tag{2}$$

$\mathcal{V}$ is the electric potential, **A** is the magnetic vector potential defined by

$$\mathbf{B}=\nabla\times\mathbf{A}, \tag{3}$$

and **B** is the magnetic field strength.

With the main device structure being formed by the electric potential $\mathcal{V}$, more subtle quantum effects can be probed by applying an external magnetic field **B**. The application of weak magnetic field allows the phase of the wave function to be altered without effecting the overall electron density distribution. For example, by applying a magnetic field to the *Aharonov-Bohm Ring*, the transmission through the ring can be made to undergo oscillations as the electron wave function constructively and destructively interferes in the output lead [4].

This paper presents a fast, accurate, and numerically stable method to solve the above time-dependent Schrödinger equation. The solution contains complete spatial and phase information of the system under study at all times, and the method can be readily applied to many theoretical studies on nanoelectronic devices operated by external electric and magnetic fields. The numerical results are compared directly to an exact analytic solution for the case of $\mathcal{V}=0$ and $\mathbf{B}=(0,0,b)$ to ensure correct propagation. Stringent numerical tests in the case of both electric and magnetic fields have also been carried out.

II. COMPUTATIONAL MODEL

As described earlier, the magnetic field enters the Hamiltonian via the vector potential **A**, i.e.,

$$\mathcal{H}=-\frac{1}{2m}(-i\nabla-e\mathbf{A})^2+e\mathcal{V}, \tag{4}$$

where **A** is defined by

$$\mathbf{B}=\nabla\times\mathbf{A}. \tag{5}$$

For a given magnetic field **B**, there are an infinite number of magnetic vector potentials **A** (namely, the different gauges), all of which provide the same results for physically measurable quantities. However, different gauges have different properties in their numerical implementation. For example, three solutions for the magnetic vector potential **A** corresponding to a constant magnetic field $\mathbf{B}=(0,0,b)$ are

$$\mathbf{A}=b(-y,0,0), \tag{6}$$

*Electronic address: stuart@physics.uwa.edu.au
†Electronic address: wang@physics.uwa.edu.au

$$\mathbf{A}=\frac{b}{2}(-y,x,0), \tag{7}$$

$$\mathbf{A}=\frac{b}{2}(x-y,x-y,0). \tag{8}$$

A closer examination shows that Eq. (7) requires the most amount of memory and computation because it has two nonzero and nonsymmetric x and y components, while Eq. (6) is not as numerically stable as Eqs. (7) and (8). The increased multiplication factor in Eq. 6, being b rather than $b/2$ for the other two gauges, doubles the size of the minute numerical error emerged from the boundaries each time the Hamiltonian is applied to the wave function. Consequently, Eq. (8) is computationally more favorable than the other two.

Once we have the magnetic vector potential $\mathbf{A}$, the system Hamiltonian $\mathcal{H}$ is set up. The Chebyshev-Fourier scheme as detailed in Ref. [6] can then be used to solve the corresponding time-dependent Schrödinger equation. Briefly, this method approximates the exponential time propagator by a Chebyshev polynomial expansion [7]

$$\psi(x,y,t)=\exp[-i(\mathcal{E}_{max}+\mathcal{E}_{min})t]\sum_{n=0}^{\mathcal{N}} a_n(\alpha) \times \phi_n(-\tilde{\mathcal{H}})\psi(x,y,0), \tag{9}$$

where $\mathcal{E}_{min}$ and $\mathcal{E}_{max}$ are the upper and lower bounds on the energies sampled by the wave packet, $a_n(\alpha)=2J_n(\alpha)$ except for $a_0(\alpha)=J_0(\alpha)$, $J_n(\alpha)$ are the Bessel functions of the first kind, and ϕ_n are the Chebyshev polynomials. To ensure convergence, the Hamiltonian needs to be normalized as

$$\tilde{\mathcal{H}}=\frac{1}{\mathcal{E}_{max}-\mathcal{E}_{min}}[2\mathcal{H}-\mathcal{E}_{max}-\mathcal{E}_{min}]. \tag{10}$$

The action of the Laplacian operator ∇ on the wave functions is carried out using a Fourier transformation technique [6].

There is a further requirement on the magnetic vector potential $\mathbf{A}$ due to the way that we evaluate the action of the Laplacian operator on the wave functions. That is, the potential should be continuous across the boundaries and preferably zero along the boundaries. This is because the Fourier transformation method, used in this work to compute derivatives, implies periodic boundary conditions [6]. As a result, any nonzero component of the wave packet crossing one boundary would reemerge on the opposite side, giving rise to unwanted artifact.

To satisfy this requirement, we define

$$\mathbf{A}=\begin{cases}(A_x(x,y),A_y(x,y),0), & x \text{ or } y \text{ not near a boundary}\\ 0, & x \text{ or } y \text{ near a boundary,}\end{cases} \tag{11}$$

which is then smoothed by convoluting with a Gaussian function or via a local averaging process. This magnetic vector potential $\mathbf{A}$ produces a constant magnetic field across the nanostructure under study but deviates from constant near the boundaries. In general, the smoothed vector potential can be expressed as

$$\mathbf{A}=(f(x,y),g(x,y),0). \tag{12}$$

Expanding Eq. (4) as

$$\mathcal{H}=-\frac{1}{2m}(-\nabla^2+ie\nabla\mathbf{A}+ie\mathbf{A}\nabla+e^2\mathbf{A}^2)+e\mathcal{V}, \tag{13}$$

leads to

$$\mathcal{H}=-\frac{1}{2m}\left(-\nabla^2+2i\hbar e\left(g(x,y)\frac{\partial}{\partial y}+f(x,y)\frac{\partial}{\partial x}\right)+i\hbar e\left(\frac{\partial f(x,y)}{\partial x}+\frac{\partial g(x,y)}{\partial y}\right)+e^2[f(x,y)^2+g(x,y)^2]\right)+e\mathcal{V}, \tag{14}$$

where $f(x,y)$ and $g(x,y)$ are smoothed functions, approximating the vector operator $\mathbf{A}$ in the region where propagation occurs, while being zero at the boundaries.

For speed of computation the components independent of ψ, that is,

$$i\hbar e\left(\frac{\partial f(x,y)}{\partial x}+\frac{\partial g(x,y)}{\partial y}\right)+e^2(f(x,y)^2+g(x,y)^2), \tag{15}$$

can be computed once and stored. While the components dependent on ψ, that is,

$$2i\hbar e\left(g(x,y)\frac{\partial}{\partial y}+f(x,y)\frac{\partial}{\partial x}\right), \tag{16}$$

must be computed each time the Hamiltonian is computed.

Evaluation of the dependent components requires six arrays to be stored ($f(x,y)$, $g(x,y)$, $\partial/\partial y$, $\partial/\partial x$ and the application of each partial derivative on the wave function) and two reverse Fourier transforms to be applied to the wave function. The net result is an increase in memory space required by seven arrays (one independent and six dependent components) and two extra reverse Fourier transforms (and the associated increase in multiplications), doubling the number of Fourier transforms computed.

The smoothing operation gives rise to moderately large spatial derivatives of the wave packet near the boundaries, which can introduce considerable numerical error if the wave packet approaches the boundary. In all calculations presented, the spatial domain is set to be sufficiently large so that the wave packet does not encounter the boundary region.

III. ANALYTIC SOLUTION

In order to verify the algorithm described above, we compare our results with the exact solution for the time evolution of an electron wave packet under the influence of a constant magnetic field with zero electric potential, i.e., $\mathbf{B}=(0,0,b)$ and $\mathcal{V}=0$. The derivation of an exact solution for the motion

of a Gaussian electron wave packet follows the work by ter Haar [8] as described below.

The Scrödinger equation for a charged particle moving in a constant uniform magnetic field is given by

$$i\hbar\frac{\partial\Psi}{\partial t}=-\frac{\hbar^2}{2m}\nabla^2\Psi+\frac{\hbar}{i}\omega_L\left(x\frac{\partial\Psi}{\partial y}-y\frac{\partial\Psi}{\partial x}\right)+\frac{1}{2}m\omega_L^2(x^2+y^2)\Psi, \tag{17}$$

where the magnetic vector potential used is $\mathbf{A}=(b/2)(-y,x,0)$ and $\omega_L=eb/2m$ is the Larmor frequency. To find a solution a rotating frame of reference is chosen

$$x=x'\cos(\omega_L t)+y'\sin(\omega_L t), \tag{18}$$

$$y=-x'\sin(\omega_L t)+y'\cos(\omega_L t), \tag{19}$$

$$t=t', \tag{20}$$

$$\Psi=\Psi'. \tag{21}$$

In this rotating frame of reference, the operators become

$$\frac{\partial}{\partial t'}=\frac{\partial}{\partial t}+\omega_L\left(x\frac{\partial}{\partial y}-y\frac{\partial}{\partial x}\right), \tag{22}$$

$$\nabla'^2=\nabla^2. \tag{23}$$

With these substitutions, the Schrödinger equation is transformed to a simple harmonic oscillator

$$i\hbar\frac{\partial\Psi'}{\partial t'}=-\frac{\hbar^2}{2m}\nabla'^2\Psi'+\frac{m\omega_L^2}{2}(x'^2+y'^2)\Psi', \tag{24}$$

with a well known solution. In two dimensions,

$$\Psi'\equiv\psi(x',y',t)=C\sum_{n,l}A_{n,l}\chi_n(\alpha x')\chi_l(\alpha y')\exp[-i\omega_L t(n+l+1)], \tag{25}$$

where $\chi_n(\alpha x)=c_n\exp(-\alpha^2x^2/2)H_n(\alpha x)$ are the eigenfunctions of the simple harmonic oscillator, $A_{n,l}=A_n^xA_l^y$ are chosen to satisfy the initial conditions with A_n^x and A_l^y referring to the x and y component of $A_{n,l}$, respectively, $H_n(\alpha x)$ are the Hermite polynomials, $\alpha=\sqrt{m\omega_L/\hbar}$ and $c_n^2=\alpha/(2^n n!\sqrt{\pi})$.

Using the generating function for the Hermite polynomials

$$\exp(-\lambda^2+2\lambda\eta)=\sum_n\frac{\lambda^n}{n!}H_n(\eta), \tag{26}$$

we have

$$\psi(x',y',0)=C\exp[-(A_n^xc_nn!)^{2/n}+2(A_n^xc_nn!)^{1/n}\alpha x']\times\exp\left[-\frac{\alpha^2x'^2}{2}\right]\exp[-(A_l^yc_ll!)^{2/l}+2(A_l^yc_ll!)^{1/l}\alpha y']\exp\left[-\frac{\alpha^2y'^2}{2}\right]. \tag{27}$$

If the initial wave packet is given by a Gaussian

$$\psi(x',y',0)=\frac{1}{\sqrt{w_xw_y\pi}}\times\exp\left(-\frac{x'^2}{2w_x^2}-\frac{y'^2}{2w_y^2}+\frac{ip_xx'}{\hbar}+\frac{ip_yy'}{\hbar}\right), \tag{28}$$

then equating the coefficients in Eqs. (27) and (28) gives

$$\frac{1}{\sqrt{w_xw_y\pi}}=C\exp[-(A_n^xc_nn!)^{2/n}-(A_l^yc_ll!)^{2/l}], \tag{29}$$

$$-\frac{1}{2w_x^2}=-\frac{\alpha^2}{2}, \tag{30}$$

$$-\frac{1}{2w_y^2}=-\frac{\alpha^2}{2}, \tag{31}$$

$$\frac{ip_x}{\hbar}=2(A_n^xc_nn!)^{1/n}\alpha, \tag{32}$$

$$\frac{ip_y}{\hbar}=2(A_l^yc_ll!)^{1/l}\alpha. \tag{33}$$

From these, we obtain the following relations:

$$w_x=w_y=\frac{1}{\alpha}, \tag{34}$$

$$A_n^xc_n=\frac{1}{n!}\left(\frac{ip_x}{2\hbar\alpha}\right)^n, \tag{35}$$

$$A_l^yc_l=\frac{1}{l!}\left(\frac{ip_y}{2\hbar\alpha}\right)^l, \tag{36}$$

$$C=\frac{\alpha}{\sqrt{\pi}}\exp\left[-\left(\frac{p_x}{2\hbar\alpha}\right)^2-\left(\frac{p_y}{2\hbar\alpha}\right)^2\right]. \tag{37}$$

The evolution of the wave packet is, therefore,

$$\psi(x',y',t)=C\sum_{n,l}\frac{1}{n!}\left(\frac{ip_x}{2\hbar\alpha}\right)^n\frac{1}{l!}\left(\frac{ip_y}{2\hbar\alpha}\right)^l \times\exp\left(-\frac{\alpha^2x'^2}{2}\right) \times\exp\left(-\frac{\alpha^2y'^2}{2}\right)H_n(\alpha x')H_l(\alpha y') \times\exp[-i\omega_L t(n+l+1)]. \quad (38)$$

By using again the generating function for the Hermite polynomials, the above expression can be further simplified as

$$\psi(x',y',t)=C\exp\left[-\lambda_x^2+2\alpha\lambda_x x'-\frac{\alpha^2x'^2}{2}-\lambda_y^2+2\alpha\lambda_y y' -\frac{\alpha^2y'^2}{2}-i\omega_L t\right], \quad (39)$$

where

$$\lambda_x=\frac{ip_x}{2\hbar\alpha}\exp(-i\omega_L t), \quad (40)$$

$$\lambda_y=\frac{ip_y}{2\hbar\alpha}\exp(-i\omega_L t). \quad (41)$$

IV. NUMERICAL RESULTS

As outlined above, there are many different potential gauge transformations that can be used. In the case of an uniform external magnetic field, we have Eqs. (6), (7), and (8). We found that all three gauges provide essentially the same time propagation of the electron wave packet. This is particularly true when a weak external magnetic field is applied to control the phase of the electron wave packet rather than greatly altering its propagation trajectory. For a large magnetic field, the selection of the gauge makes a slight difference to the propagation error. It is found that calculations using Eqs. (7) and (8) are more accurate than using Eq. (6). This is due to, as discussed above, the half of b in these equations, which reduces errors emerged from the boundaries each time the Hamiltonian is applied. Due to the linearity of the Chebyshev propagation scheme, applying the Hamiltonian N times with error δ results in a total error for the summation of $O(N\delta)$. Consequently, for a typical run with 1000 terms in the summation, Eq. 6 can have an error 1000 times greater than the other two gauges. However, it was still found to be typically below 10^{-6}. In terms of efficiency, the symmetric gauge [i.e., Eq. (8)] is simpler to implement and produces faster and more economical codes than Eq. (7). This gauge is therefore used for the calculations reported below.

A second consideration is the requirement that the vector potential **A** be continuous across the boundaries and preferably zero along the boundaries, since the Fourier transformation method is used to compute the derivatives [1]. Also, to reduce high frequency noise, the vector potential should be smooth, without sharp spikes especially near the boundaries. This has been achieved by imposing the condition that the vector potential smoothly drops to zero at the boundaries. The x and y component of **A** used in this work are plotted in Figs. 1(a) and 1(b), respectively. As shown the vector potential is symmetric in the x and y directions. It is also continuous, smooth, and zero across the boundaries.

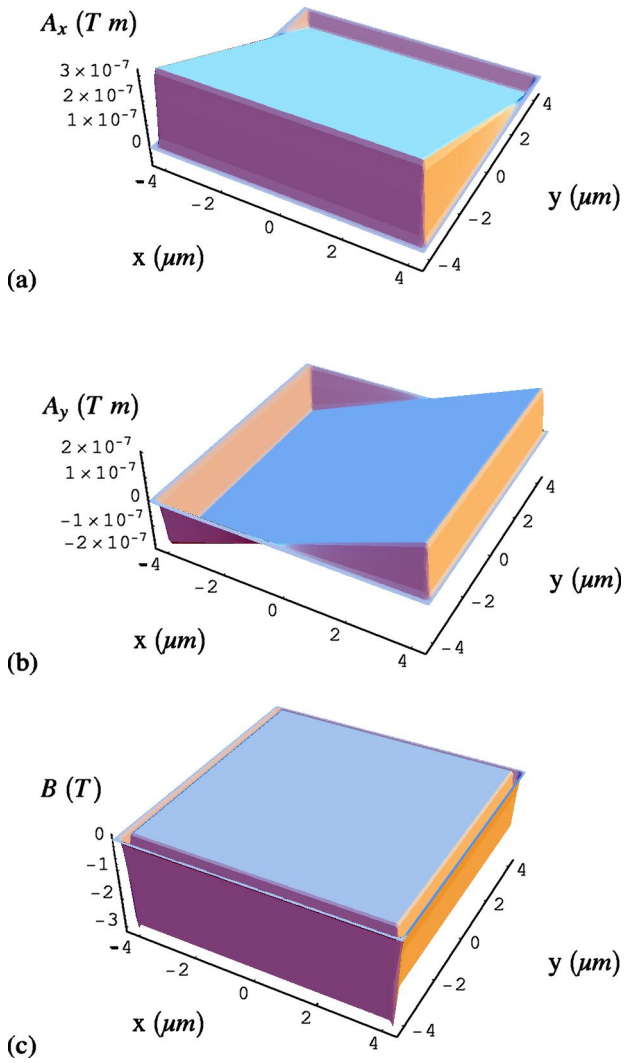

FIG. 1. (a) and (b) The x and y components of the vector potential **A** used in this work; (c) the magnetic field produced from this vector potential using Eq. (5). The spatial size of the simulation is 8 μm in each dimension.

From the magnetic vector potential **A**, the effective magnetic field can be calculated by Eq. (5). Although the smoothing operation on the vector potential **A** alters its function form as given in Eq. (11), Fig. 1(c) demonstrates that in the region where the wave packet is propagating, the correct uniform magnetic field $\mathbf{B}=(0,0,0.1\ \mathrm{T})$ is experienced. It is only when the wave packet approaches the boundaries that it would experience a nonuniform magnetic field. This is ensured not to happen by setting up a sufficiently large numerical grid, so that the wave packet is sufficiently away from the boundaries throughout the entire propagation.

Great care must be taken when including the magnetic

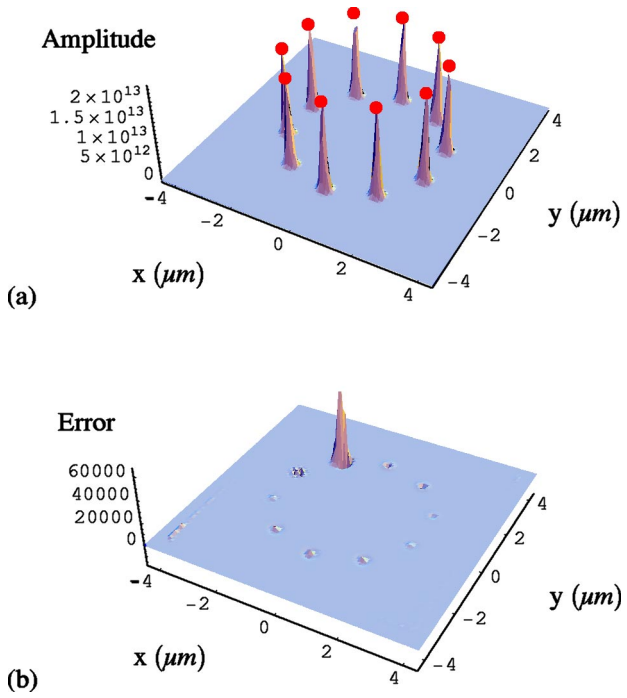

FIG. 2. (a) Propagation of an electron wave packet under the influence of the magnetic field shown in Fig. 1(c). The circles above the wave packet indicate the classical particle trajectory. (b) Absolute errors between our numerical results and the analytic solution.

fields in the Hamiltonian, as the momentum of the wave packet can be transformed from the x direction into the y direction. If the numerical grid is not set up correctly, for example, if each dimension supports a different maximum momentum, high frequency noise can be effected leading to numerical instability. Also, the change in momentum from the x to y dimension results in a high maximum momentum being required to track. This can be taken care of by adjusting the scaling of the Hamiltonian in the Chebyshev propagation scheme such as increasing $\mathcal{E}_{max}$, the upper bound on the energies sampled by the wave packet.

Figure 2(a) shows that the electron wave packet follows the same trajectory as a classical electron in the same magnetic field. The wave packet initially has energy 0.082 eV in the x direction and momentum spread 2.3%. The propagation is under the influence of an applied magnetic field of 0.1 T. The time step is chosen to be 0.023 ps, so a full circle takes 0.23 ps. The absolute error between our numerical solution obtained using the Chebychev-Fourier scheme and the analytic solution given by Eq. (39) is shown in Fig. 2(b). The maximum error is about one part in a billion, which is close to machine accuracy.

Since the Schrödinger equation is symmetric with respect to time reversal, a stringent test of reliability of the solution is to reverse the evolution with time and the wave function should return to its initial state. If errors were accumulated along the way, a reverse propagation would lead to something quite different from the starting wave function. This test was performed by propagating the initial wave function forward and then backward in time as shown in Fig. 3. In this case, apart from the constant magnetic field of 0.1 T, a

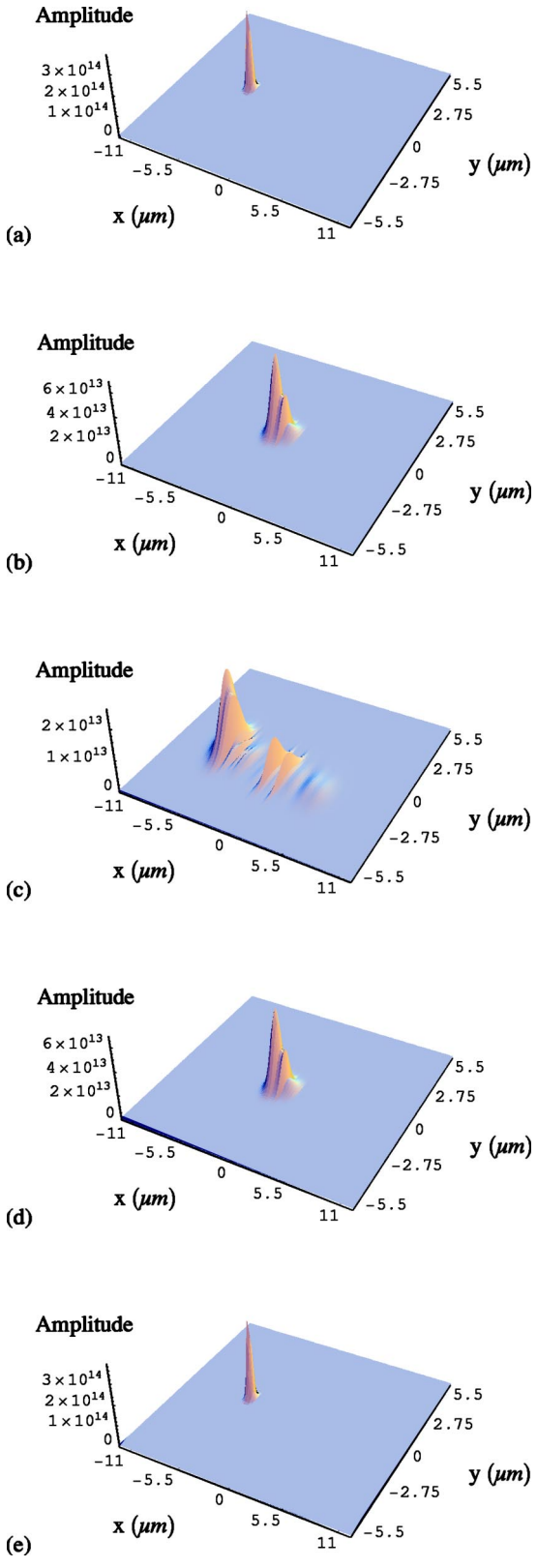

FIG. 3. (a)–(c) The forward-time propagation of the wave packet through a double electric potential barrier under a constant magnetic field. Parts (d) and (e) show the backward-time propagation of the wave packet to reform the initial wave packet.

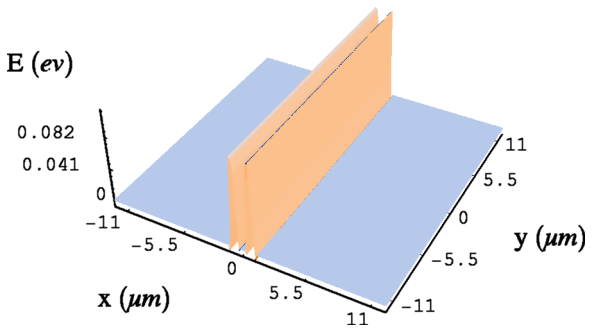

FIG. 4. The double electric potential barrier with height of 0.082 eV.

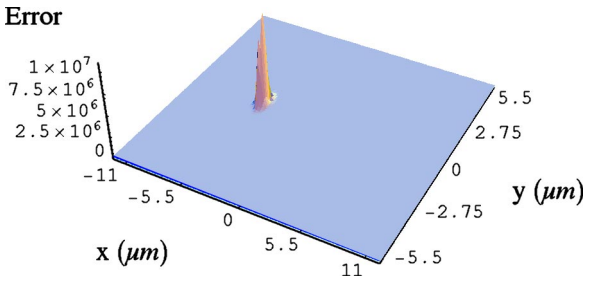

FIG. 5. Error between the initial wave packet and the foward-backward time propagated wave packet. This error is 7 to 8 orders of magnitude smaller than the wave packet, indicating that the propagation method introduces little error.

double electric potential barrier as shown in Fig. 4 is also applied so that the electron wave packet propagates under the influence of both electric and magnetic field. The initial wave packet has energy of 0.082 eV and 10% momentum spread. The time step between each snap shot is 0.4 ps. The error between the initial wave packet and the forward-then-backward propagated wave packet is shown in Fig. 5. The maximum error is again extremely small, in the order of 10^{-8}.

In addition, we found that both the energy and the norm were conserved to the order of 10^{-8} through all the calculations. These tests provide strong evidence that our computational model is highly accurate, while maintaining the full quantum information.

The method described above is applicable to more than just uniform constant magnetic fields. As long as an appropriate vector potential can be constructed, arbitrary magnetic fields can be studied. By smoothing the vector potentials at the boundary, the computation should proceed with little error, as with the results shown in this paper. While the Chebyshev propagation scheme is only valid for time-independent potentials, time-dependent magnetic fields may be studied by using many small time steps, considerably smaller than the oscillation of the magnetic field. In this fashion, the method demonstrated is extensible to arbitrarily shaped and time varying magnetic fields.

The above calculations were performed on a single 1 GHz alpha processor with 1 GB of memory. The results for Figs. 2 and 3 consumed about 18 and 21 h of CPU time, respectively. The memory requirement is about 500 MB. These calculations are considerably longer than normally required in order to demonstrate its numerical stability and accuracy. We have also performed detailed calculations for the experimental set up of Koonan *et al.* [1], which took about 4 h of CPU time on the same computer. This will be reported in a separate publication.

V. CONCLUSION

Presented in this paper is a fast, accurate, and numerically stable computational scheme for the time-dependent propagation of an electron wave packet under the influence of both electric and magnetic fields. The algorithm is based on direct numerical integration of the time-dependent Schrödinger equation. This is an extension of our earlier work on electron transport governed by electric potentials [1]. Stringent tests on the accuracy of our solutions were carried out, including conservation of norm and energy, time reversal propagation, and comparison with exact solutions in the case of constant uniform magnetic field with zero electric potential. This model can be readily applied to arbitrarily complex magnetic field profiles as well as time-varying external fields. It is anticipated that such a scheme will prove useful for studying systems such as quantum ratchets, Aharonov-Bohm ring, magnetic and electric impurities, quantum chaos, as well as various quantum interference phenomena.

[1] J.J. Koonen, H. Buhmann, and L.W. Molenkamp, Phys. Rev. Lett. **84**, 2473 (2000).
[2] H. Linke, W.D. Sheng, A. Svensson, A. Lofgren, L. Christensson, H.Q. Xu, and P. Omling, Phys. Rev. B **61**, 15 914 (2000).
[3] R. Narevich, R.E. Prange, and O. Zaitsev, Phys. Rev. E **62**, 2046 (2000).
[4] M. Entin and M. Mahmoodian, J. Phys.: Condens. Matter **12**, 6845 (2000).
[5] B.L. Gallagher *et al.*, Acta Phys. Pol. A **98**, 217 (2000).
[6] J.B. Wang and S. Midgley, Phys. Rev. B **60**, 13 668 (1999).
[7] H. Tal-Ezer and R. Kosloff, J. Chem. Phys. **81**, 3967 (1984).
[8] D. ter Haar, *Problems in Quantum Mechanics* (Pion, London, 1975).